

PCCP

Accepted Manuscript



This is an *Accepted Manuscript*, which has been through the Royal Society of Chemistry peer review process and has been accepted for publication.

Accepted Manuscripts are published online shortly after acceptance, before technical editing, formatting and proof reading. Using this free service, authors can make their results available to the community, in citable form, before we publish the edited article. We will replace this *Accepted Manuscript* with the edited and formatted *Advance Article* as soon as it is available.

You can find more information about *Accepted Manuscripts* in the [Information for Authors](#).

Please note that technical editing may introduce minor changes to the text and/or graphics, which may alter content. The journal's standard [Terms & Conditions](#) and the [Ethical guidelines](#) still apply. In no event shall the Royal Society of Chemistry be held responsible for any errors or omissions in this *Accepted Manuscript* or any consequences arising from the use of any information it contains.

Can a Single Water Molecule Really Affect the Hydrogen Abstraction Reaction of HO₂+NO₂ under Tropospheric Conditions?

Tianlei Zhang^{a,*}, Rui Wang^a, Hao Chen^a, Suotian Min^a, Zhiyin Wang^a, Caibin Zhao^a, Qiong Xu^a, Lingxia Jin^a, Wenliang Wang^{b,*}, Zhuqing Wang^c

^a School of Chemical & Environment Science, Shaanxi University of Technology, Hanzhong, Shaanxi 723001, China

^b Key Laboratory for Macromolecular Science of Shaanxi Province, School of Chemistry & Chemical Engineering, Shaanxi Normal University, Xi'an, Shaanxi 710062, China

^c Shandong Provincial Key Laboratory of Ocean Environment Monitoring Technology, Shandong Academy of Sciences Institute of Oceanographic Instrumentation, Qingdao 266001, China.

Abstract

The effect of a single water molecule on the hydrogen abstraction reaction of HO₂ + NO₂ has been investigated by employing B3LYP and CCSD(T) theoretical approaches in connection with the aug-cc-pVTZ basis set. The reaction without water has three kinds of reaction channels on both singlet and triplet potential energy surfaces depending on how the HO₂ radical approached NO₂, corresponding to the formation of *trans*-HONO+O₂, *cis*-HONO+O₂ and HNO₂+O₂. Our calculated results show that triplet reaction channels are favorable and their total rate constant, at 298 K, is $2.01 \times 10^{-15} \text{ cm}^3 \cdot \text{molecule}^{-1} \cdot \text{s}^{-1}$ in good agreement with experimental values. A single water molecule affects each one of these triplet reaction channels in three different reactions of H₂O⋯HO₂+ NO₂, HO₂⋯H₂O+ NO₂ and NO₂⋯H₂O+ HO₂, depending on the way the water interacts. Interestingly, the water molecule in these reactions not only acts as a catalyst giving the same products as the naked reaction, but also as a reactant giving the product of HONO₂+H₂O₂. The total rate constant of H₂O⋯HO₂+ NO₂ reaction is estimated to be slower than the naked reaction by 6 order of magnitude at 298 K. However, the total rate constant of HO₂⋯H₂O+ NO₂ and NO₂⋯H₂O+ HO₂ reaction is respectively faster than the naked reaction by 4 and 3 orders of magnitude at 298 K, and their total effective rate constant is predicted to be 1.2 times than the corresponding total rate constant without water at 298 K, which is agreement with the predication reported by Li et al (*science*, 2014, **344**, 292-296).

Key words: HO₂; Dual level direct dynamics; Water Effect; Tropospheric Conditions

* Corresponding authors. Tel: +86-0916-2641083, Fax: +86-0916-2641083.

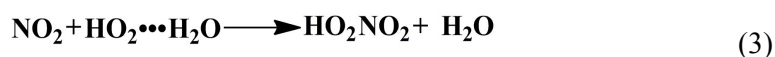
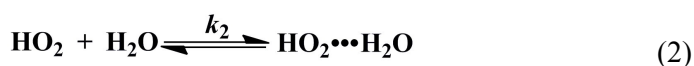
e-mail: ztianlei88@163.com (T. L. Zhang); wlwang@snnu.edu.cn (W. L. Wang).

1. Introduction

Water has a very significant impact on the processes that occur in the Earth's atmosphere^[1]. It can form hydrogen-bonded complexes with many atmospheric species such as ozone, nitrogen acids, sulphuric acid and chlorine oxides, changing their photochemical features, and it can even participate actively in atmospheric reactions producing a catalytic effect^[2-5]. Furthermore, water vapor can have hydrogen-bond interactions with other reactive atmospheric species, modifying the stability of pre-reactive complexes and of the transition states and therefore having a direct impact on reaction kinetics^[6-8]. Thus, for instance, water forms hydrogen-bonded complexes with the hydroperoxyl radical, which enhances the HO₂ self-reaction producing H₂O₂ and O₂.^[9-12]



The kinetics of reaction (1) has been extensively studied experimentally and theoretically for the given range of temperatures and pressures.^[13-17] As the formation of HO₂NO₂ is similar to the HO₂ self-reaction, the water effect on reaction (1a) has been investigated by Sander and Peterson^[18]. Similar to the HO₂ self-reaction, a significant enhancement in the rate was observed in Sander and Peterson's report when water vapor was added. A negative temperature dependence on the rate is also seen in this report, as the effective third-order rate constant increases from 1.0×10^{-30} to 1.6×10^{-30} as the temperature decreases from 298 to 275 K. Besides, they postulated possible catalytic mechanism (Reaction (2) and (3)) for reaction (1a).



Latter, the reaction of reaction (1a) without and with water vapor has been studied theoretically via ab initio methods^[19]. It was found that the rate for reaction (3) was found to be $4.7 \times 10^{-30} \text{ cm}^6 \cdot \text{molecule}^{-2} \cdot \text{s}^{-1}$, which is approximately 200 times faster than the calculated rate of reaction (1a) and 25 times faster than the experimentally suggested rate for reaction (1a). This reaffirms that the introduction of water enhance the rate of reaction (1a). All these experimental and theoretical investigations above, provides meaningful information to the mechanism and kinetics of HO₂ + NO₂ reaction under tropospheric conditions. However, for reaction (1b), the investigation of the water effect is scarce, despite this reaction also remove the reactive radicals

HO₂ and NO₂ and may provide sinks for both the HO_x and NO_x species^[20, 21]. To our best of our knowledge, there is only one theoretical report for the water effect on the title reaction has been reported by Staikova et al^[22]. Dissimilar to water effect of reaction (1a) in Aloisio's study^[19], Staikova et al^[22] demonstrated that a single water molecule does not alter the barrier height to reaction (1b) by calculating double hydrogen transfer mechanism for HO₂NO₂···H₂O→HONO···H₂O+O₂ reaction. Although Staikova et al^[22] proved that the water molecule in reaction (1b) acts as a catalyst giving the same products as the naked reaction, reactions of H₂O···HO₂+ NO₂, HO₂···H₂O+ NO₂ and NO₂···H₂O+ HO₂ in the presence of a water molecule and the water molecule in this reactions as a reactant giving the product of HONO₂+H₂O₂ have not been involved. Thus it is still difficult to judge whether a single water molecule really not affect the hydrogen abstraction reaction of reaction (1b) under tropospheric conditions is reasonable or not. In addition, recently the mechanism of HO₂···H₂O+ NO₂ has been postulated as an important HONO source reported by Li et al^[23]. Thus, it is necessary to study the reaction mechanism and rate constant for HO₂+ NO₂ reaction with a water molecule to produce HONO formation in detail for the purpose of a better understanding of the effects of water vapor on hydrogen abstraction reaction of HO₂ + HO₂ under tropospheric conditions.

In the present study, a detailed water effect on hydrogen abstraction reaction of HO₂ + NO₂ to produce HONO formation is carried out at the CCSD(T)/aug-cc-pVTZ //B3LYP/aug-cc-pVTZ level of theory, which is organized as follows: firstly, hydrogen abstraction reaction of HO₂ + NO₂ is investigated to compare with water-catalyzed processes. Then the reactions of H₂O···HO₂+ NO₂, HO₂···H₂O+ NO₂ and NO₂···H₂O+ HO₂ in the presence of a water molecule where water molecule acts as a catalyst, as well as the reactions that water molecule as a reactant are evaluated by investigating direct hydrogen abstraction process and double hydrogen transfer mechanisms. Finally, the theoretical rate constants of the most favorable primary channel are calculated to investigate the atmospheric relevance of water molecule's effect. Overall, this work may lead to a better understanding of the effects of water vapor on gas-phase reactions under tropospheric conditions.

2. Computational Methods

The quantum chemistry calculations reported in this work were carried out with Gaussian

03^[24] program packages. We used the B3LYP method with the aug-cc-pVTZ basis set to optimize and characterize all stationary points investigated in this work. At this level of theory, we also calculated the harmonic vibrational frequencies to verify the nature of the corresponding stationary points (minima or transition state), to provide the zero-point vibrational energy (ZPE) and to determine the thermodynamic contributions to the enthalpy and free energy. Moreover, to ensure that the transition states were connected to the desired reactants and products, we performed intrinsic reaction coordinate (IRC) calculations. In order to obtain more accurate relative energies, we performed single-point CCSD(T)^[25] calculations at the optimized geometries using the aug-cc-pVTZ basis set. Furthermore, in order to check the reliability of single-determinant-based methods, we looked at the T_1 diagnostic^[26-30] in the CCSD wave function with regards to the multireference character of the wave function. The T_1 diagnostic values of the closed-shell and open-shell stationary points shown in Table S1† were less than 0.02 and 0.042, respectively, revealing that the multireference character of the CCSD(T) wave functions was not a problem, and that the CCSD wave functions in this study were reliable. Finally, the kinetic properties of the system were calculated using conventional transition state theory (TST)^[31-33] in the VKLab program^[34] coupled with the steady state approximation. These calculations made use of the energies obtained at the CCSD(T)/aug-cc-pVTZ//B3LYP/aug-cc-pVTZ level of theory and the partition functions computed at the B3LYP/aug-cc-pVTZ level of theory. The tunnelling correction to the rate constants was computed using the zero-order approximation of a vibrationally adiabatic potential energy surface (PES) with zero curvature. In this case, the unsymmetrical Eckart potential energy barrier was used to approximate the potential energy curve. Details about the geometric parameters, the relative energies, enthalpies and free energies of the stationary points investigated as well as the rate constants are reported in the Supporting Information.

3. Results and Discussions

The transition states in each reaction channel were denoted by “TS” followed by a number, and intermediates were denoted by “IM” followed by a number. The letter “a” was used to distinguish the transition states and pre-reactive intermediates that were conformers of each other and therefore had the same features; a species in the presence of a water molecule was denoted by a “W” prefix.

3.1 Potential energy surfaces for hydrogen abstraction reaction of NO₂+HO₂

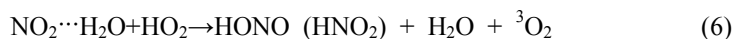
Regarding the hydrogen abstraction reaction of NO₂+HO₂ to produce HONO formation, three kinds of reaction channels were identified on both singlet and triplet potential energy surfaces depending on how the HO₂ radical approached NO₂, corresponding to the formation of *trans*-HONO+O₂, *cis*-HONO+O₂ and HNO₂+O₂. In accordance with the result of Staikova et al [22], the singlet channels are negligible for their high barriers. Therefore, Fig. 1 displays the schematic energy diagrams of the low-energy routes for the triplet hydrogen abstraction reaction of NO₂+HO₂, whereas the schematic energy diagrams for other singlet and triplet hydrogen abstraction channels are respectively shown in Fig. S2 and S4.

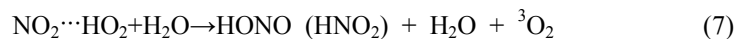
Regarding to HONO+³O₂ formation, two reaction channels R1 and R2 were identified, depending on how the HO₂ radical approached NO₂, corresponding to the *cis*-HONO+³O₂ and *trans*-HONO+³O₂. As seen in Fig. 1, a weak hydrogen bond between the H atom of HO₂ and one O atom of NO₂ (with a computed O...H bond distance of 2.033 and 1.940 Å at the B3LYP/aug-cc-pVTZ level of theory) was present in IMA and IMb, which likely explained why the relative energy of IMA and IMb to the reactants (HO₂ and NO₂), shown in Fig. 1 and Table S2, was only -1.92 and -2.64 kcal·mol⁻¹. Starting from IMA and IMb, one O atom of NO₂ attacked the H atom of HO₂ through the *cis*-transition states of TSa and TSb. From an energetic standpoint, Fig. 1 and Table 1 show that at 0 K, the two transition states TS1 and TS1a were predicted to be, respectively, 13.36 and 13.75 kcal·mol⁻¹ above the energies of the reactants.

Differently from Channels R1 and R2 that begin with the formation of pre-reaction hydrogen bonded complexes before the transition states and the formation of the products, the reaction of Channel R3 went on directly through the transition state TSc occurring by the N atom of NO₂ attacks the H atom of HO₂. From an energetic point of view, Fig. 1 and Table S2 show that at 0 K, the relative energy of TSc was predicted to be 8.36 kcal·mol⁻¹ to the reactants, which was 4.03 and 0.65 kcal·mol⁻¹ less than the corresponding value of TSa and TSb to the reactants. These results indicate that HNO₂+³O₂ (Channel R3) was easily taken place for the title reaction when a water molecule was not present.

3.2 Potential energy surfaces for hydrogen abstraction reaction of NO₂+HO₂ with a water molecule

As seen the hydrogen abstraction reaction of NO₂+HO₂ above, the singlet channels are negligible. So herein the impact of water on the triplet hydrogen abstraction reaction of NO₂+HO₂ is only considered. The addition of water molecule makes the triplet hydrogen abstraction reaction of NO₂+HO₂ much more complex leading to the four following bimolecular reactions:





The significance of these reactions depends on the extent to which the respective bimolecular complexes, $\text{H}_2\text{O} \cdots \text{HO}_2$, $\text{HO}_2 \cdots \text{H}_2\text{O}$, $\text{NO}_2 \cdots \text{H}_2\text{O}$ and $\text{NO}_2 \cdots \text{HO}_2$ exist, which can be determined by computing their stability and corresponding equilibrium constants. $\text{H}_2\text{O} \cdots \text{HO}_2$ forms a five-membered ring-like structure via the formation of two hydrogen bonds where both HO_2 radical and H_2O act as hydrogen donor and acceptor or simultaneously as seen in Fig. 2. The bonding energy of $\text{H}_2\text{O} \cdots \text{HO}_2$ was $6.73 \text{ kcal}\cdot\text{mol}^{-1}$, which agrees well with previously reported values.^[8, 10] $\text{HO}_2 \cdots \text{H}_2\text{O}$, $\text{NO}_2 \cdots \text{HO}_2$ and $\text{NO}_2 \cdots \text{H}_2\text{O}$ were less stable complex than $\text{H}_2\text{O} \cdots \text{HO}_2$ with a single hydrogen bond involved.

The equilibrium constants of these complexes at 298 K are 5.67×10^{-19} , 1.57×10^{-23} , 2.50×10^{-23} and $3.69 \times 10^{-24} \text{ cm}^3\cdot\text{molecule}^{-1}$, respectively (Table 1). Taking into account typical tropospheric concentrations of $7.64 \times 10^{17} \text{ molecules}\cdot\text{cm}^{-3}$ of H_2O , $3 \times 10^8 \text{ molecules}\cdot\text{cm}^{-3}$ of HO_2 ,^[35] and $10^9 \text{ molecules}\cdot\text{cm}^{-3}$ of NO_2 , it is estimated that the atmospheric concentration of the $\text{H}_2\text{O} \cdots \text{HO}_2$ complex to be $1.30 \times 10^{10} \text{ molecules}\cdot\text{cm}^{-3}$, the concentration of the $\text{HO}_2 \cdots \text{H}_2\text{O}$ and $\text{NO}_2 \cdots \text{H}_2\text{O}$ complex is estimated to be 3.50×10^5 and $1.91 \times 10^6 \text{ molecules}\cdot\text{cm}^{-3}$. Whereas the concentration of $\text{NO}_2 \cdots \text{HO}_2$ is negligible ($1.11 \times 10^{-6} \text{ molecules}\cdot\text{cm}^{-3}$), and therefore reaction 7 will not be considered, and the $\text{H}_2\text{O} \cdots \text{HO}_2 + \text{NO}_2$, $\text{HO}_2 \cdots \text{H}_2\text{O} + \text{NO}_2$ and $\text{NO}_2 \cdots \text{H}_2\text{O} + \text{HO}_2$ reactions will be the focus of the remainder of this article for the impact of water on the triplet hydrogen abstraction reaction of $\text{NO}_2 + \text{HO}_2$.

3.2.1 Potential energy surfaces of $\text{H}_2\text{O} \cdots \text{HO}_2 + \text{NO}_2$ reaction

For the $\text{H}_2\text{O} \cdots \text{HO}_2 + \text{NO}_2$ reaction in Fig. 3, the products of *trans*- $\text{HONO} \cdots \text{H}_2\text{O} + {}^3\text{O}_2$, *cis*- $\text{HONO} \cdots \text{H}_2\text{O} + {}^3\text{O}_2$ and $\text{HNO}_2 \cdots \text{H}_2\text{O} + {}^3\text{O}_2$ can be obtained transferring hydrogen atom through a water molecule from HO_2 radical to NO_2 . In another words, similar with other water-catalyzed reactions before^[11, 12, 36], the influence of a single water molecule occurring through $\text{H}_2\text{O} \cdots \text{HO}_2 + \text{NO}_2$ reaction has been investigated by taking into account double hydrogen transfer mechanism.

Fig. 3 displays the double hydrogen transfer mechanism (Channels RW1a, RW2a and RW3a) for the formation of ${}^3\text{O}_2$ occurring through $\text{H}_2\text{O} \cdots \text{HO}_2 + \text{NO}_2$ reaction. Channel RW3a may be negligible for the high relative energy ($9.20\text{-}15.46 \text{ kcal}\cdot\text{mol}^{-1}$) of its transition state TSW3a (TSW3a1) to the transition states of TSW1a (TSW1a1) and TSW2a (TSW2a1) respectively in

Channels RW1a and RW2a. Such barrier discrepancy was possibly due to that the Mulliken atomic charges of N atom in NO₂ was 0.54 compared with that of O atom in NO₂ was -0.27 at the B3LYP/aug-cc-pVTZ level, which makes the hydrogen abstraction reaction abstracted by O atom of NO₂ from the O atom of water molecule is much easier than that abstracted by N atom of NO₂ from the O atom of water molecule.

Regarding to Channel RW1a, Fig. 3(a) shows that, beginning with the H₂O⋯HO₂+NO₂ reactants, the first step of Channel RW1a involves a formation of hydrogen bond complex IMW1a and IMW1a1. The computed binding energy of IMW1a and IMW1a1 is respectively 0.90 and 0.98 kcal·mol⁻¹. Both IMW1a and IMW1a1 complexes have two hydrogen bonds, the first between the H atom of HO₂ and the O atom of water, and the second one between one H atom of water and the O(1) atom of NO₂. After the prereactive complexes of IMW1a and IMW1a1, Channel RW1a goes on through double hydrogen transfer elementary reaction (TSW1a and TSW1a1) and the transition state of TSW1a and TSW1a1 lay 21.79 and 21.60 kcal·mol⁻¹ above the reactants of H₂O⋯HO₂+NO₂. It was noteworthy that the geometrical structures both of the intermediates (IMW1a and IMW1a1) and the transition states (TSW1a and TSW1a1) were mainly differing in the relative orientations of the dangling hydrogen atoms. These differences were distinguished from each other by the dihedral angle of ∠O(3)-H(5)-O(4)-H(7) (130.7° and -111.4° for IMW1a and IMW1a1, respectively, whereas 138.5° and -138.5° for TSW1a and TSW1a1, respectively). Compared with the corresponding non-catalytic Channel, Channel R1, the barrier height of Channel RW1a is higher by 9.49-9.68 kcal·mol⁻¹ than that of Channel R1, indicating that the single water molecule has negative influence on the reaction barrier of *trans*-HONO +³O₂ formation occurring through H₂O⋯HO₂+NO₂ reaction.

Similar to Channel RW1a (Fig. 3(a)), Fig. 3(b) shows that, starting from H₂O⋯HO₂+NO₂ reactants, two pathways including TSWb and TSWb1 have been identified for Channel RW2a and we found that, for these two pathways, the relative energies both of the intermediates (-2.80 kcal·mol⁻¹ for IMW2a, -2.75 kcal·mol⁻¹ for IMW2a1) and the transition states (15.55 kcal·mol⁻¹ for TSW2a, 15.56 kcal·mol⁻¹ for TSW2a1) to the reactants (H₂O⋯HO₂+NO₂) were close to each other at the CCSD(T)/aug-cc-pVTZ//B3LYP/aug-cc-pVTZ level of theory because of the similarity in their configuration. Compared with the barrier height of Channel

R2 (Fig. 1), the relative energy of TSW2a and TSW2a1 to the $\text{H}_2\text{O}\cdots\text{HO}_2+\text{NO}_2$ reactants is higher by $6.44\text{ kcal}\cdot\text{mol}^{-1}$ than that of TSb to the HO_2+NO_2 reactants, indicating that, similar with Channel RW1a, the single water molecule in Channel RW2a has negative influence on reducing the reaction barrier of *cis*-HONO + $^3\text{O}_2$ formation occurring through $\text{H}_2\text{O}\cdots\text{HO}_2+\text{NO}_2$ reaction.

3.2.2 Potential energy surfaces for $\text{HO}_2\cdots\text{H}_2\text{O} + \text{NO}_2$ reaction

The water molecule in $\text{HO}_2\cdots\text{H}_2\text{O} + \text{NO}_2$ reaction not only acts as a catalyst (Fig. 4) giving the same products as the naked reaction, but also as a reactant (Fig. 5) giving the product of $\text{HONO}_2+\text{H}_2\text{O}_2$. As seen from Fig. 4, the products *trans*-HONO+ $\text{H}_2\text{O} + ^3\text{O}_2$ (Channel RW1b), *cis*-HONO+ $\text{H}_2\text{O} + ^3\text{O}_2$ (Channel RW2b) and $\text{HNO}_2+\text{H}_2\text{O} + ^3\text{O}_2$ (Channel RW3b) can be obtained through direct hydrogen abstraction process, as described before^[6, 8, 35, 37-41], whereas the product of $\text{HONO}_2+\text{H}_2\text{O}_2$ (Channel RW4) in Fig. 5 can be obtained occurring through addition-hydrogen abstraction reaction.

Regarding to the Channels RW1b and RW2b, it can be seen in Fig. 4 that two hydrogen bond complex (IMW1b, Channel RW1b; IMW2b, Channel RW2b) including the mirror structures have been identified. The energies of the two hydrogen bond complex relative to the reactants of $\text{HO}_2\cdots\text{H}_2\text{O}+\text{NO}_2$ are close to each other at the CCSD(T)/aug-cc-pVTZ//B3LYP/aug-cc-pVTZ level, from 2.65 to $3.71\text{ kcal}\cdot\text{mol}^{-1}$. However, IMW2b is more stable than IMW1b. For the transition states of Channels RW1b and RW2b, in geometrical point of view, both TSW1b and TSW2b follow the direct hydrogen abstraction. Take TSW1b as an example, the H atom of HO_2 moiety in $\text{HO}_2\cdots\text{H}_2\text{O}$ complex migrates to one O atom of NO_2 to produce *trans*-HONO+ $\text{H}_2\text{O} + ^3\text{O}_2$, suggesting a one-hydrogen-transfer event. From an energetic point of view, the relative energy of TSW1b in Fig.4(b) is above the $\text{H}_2\text{O}\cdots\text{HO}_2 + \text{NO}_2$ reactants by $12.24\text{ kcal}\cdot\text{mol}^{-1}$, which is higher by $2.73\text{ kcal}\cdot\text{mol}^{-1}$ than that of TSW2b, so Channel RW2b is favorable than Channel RW1b. Moreover, compared with Channels RW1a and RW2a in Fig. 3, the barrier height of Channels RW1b and RW2b is lower by 5.52 and $12.18\text{ kcal}\cdot\text{mol}^{-1}$, respectively, indicating that, for water-catalyzed channel 1 and 2, Channel RW1b and RW2b is favorable than the corresponding Channel of Channel RW1a and RW2a.

Regarding to the Channel RW3b shown in Figure 4(c), beginning with the $\text{HO}_2\cdots\text{H}_2\text{O} + \text{NO}_2$ reactants, the reaction progressed through the transition state TSW3b undergoing a direct

hydrogen abstraction process by the N atom of NO_2 radical abstracted the H atom of HO_2 moiety in the $\text{HO}_2\cdots\text{H}_2\text{O}$ complex. From an energetic point of view, outlined in Fig. 4 and Table S4, the relative energies of the transition state TSW3b was $7.81 \text{ kcal}\cdot\text{mol}^{-1}$ above the $\text{H}_2\text{O}\cdots\text{HO}_2 + \text{NO}_2$ reactants, which was $\sim 23.20 \text{ kcal}\cdot\text{mol}^{-1}$ less than the relative energies associated with the transition state TSW3a involved in Channel RW3a, showing that for water-catalyzed channel R3, Channel RW3b is favorable than the corresponding Channel of Channel RW3a. As a result, which has been discussed above that water molecule as a catalyst, the channels involved in the $\text{HO}_2\cdots\text{H}_2\text{O} + \text{NO}_2$ reaction is favorable than the corresponding channel involved in the $\text{H}_2\text{O}\cdots\text{HO}_2 + \text{NO}_2$ reaction.

Fig. 5 shows the schematic potential energy surface for the reaction between $\text{HO}_2\cdots\text{H}_2\text{O}$ and NO_2 leading to the formation of $\text{HNO}_3 + \text{H}_2\text{O}_2$ (Channel RW4). As seen from Fig. 5, starting from the $\text{HO}_2\cdots\text{H}_2\text{O} + \text{NO}_2$ reactants, the reaction goes on through TSW4b and TSW4b1 in a process that involves the formation of a covalent N–O(H) bond and simultaneously, a hydrogen atom transfer from the water moiety to the terminal O atom of the HO_2 moiety. The computed energy barrier is 26.73 and $27.85 \text{ kcal}\cdot\text{mol}^{-1}$ and the process leads to the formation of IMFW4b and IMFW4b1, which is predicted to lie 18.03 and $22.08 \text{ kcal}\cdot\text{mol}^{-1}$ below the energy of the $\text{H}_2\text{O}\cdots\text{HO}_2 + \text{NO}_2$ reactants. IMFW4b and IMFW4b1 are hydrogen bonded complexes formed between HNO_3 and H_2O_2 , so that this is a new mechanism for the gas-phase formation of HNO_3 . Compared with the barrier height of other Channels (Channels RW1b, RW2b and RW3b) of $\text{HO}_2\cdots\text{H}_2\text{O} + \text{NO}_2$ reaction in Fig. 4, the relative energy of TSW4b and TSW4b1 to the $\text{H}_2\text{O}\cdots\text{HO}_2 + \text{NO}_2$ reactants is higher by 14.63 – $18.20 \text{ kcal}\cdot\text{mol}^{-1}$. However, the results of the present section lead us to conclude that water introduces different features with respect to the naked reaction, acting as a reactant, but also producing a new reactivity.

3.2.3 Potential energy surfaces for $\text{NO}_2\cdots\text{H}_2\text{O} + \text{HO}_2$ reaction

A potential energy surface for water-catalyzed $^3\text{O}_2$ formation occurring through $\text{NO}_2\cdots\text{H}_2\text{O} + \text{HO}_2$ reaction can be seen in Fig. 6. It can be seen from Fig. 6(a) and 6(b) that the hydrogen atom of the HO_2 radical abstracted by the terminal oxygen atom of NO_2 moiety in $\text{NO}_2\cdots\text{H}_2\text{O}$ complex with the prereactive complex IMW1c and IMW2c involved. Both complexes IMW1c and IMW2c had two hydrogen bonds, the first between the hydrogen atom of HO_2 and the terminal oxygen atom of NO_2 moiety in $\text{NO}_2\cdots\text{H}_2\text{O}$ complex, the second between one hydrogen

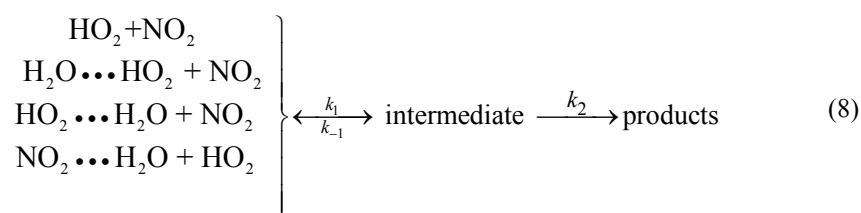
atom of H₂O moiety in NO₂···H₂O complex and the oxygen atom of NO₂ moiety in NO₂···H₂O complex. The relative energy of complex IMW1c and IMW2c to the NO₂···H₂O+HO₂ reactants was -7.68 and -2.49 kcal·mol⁻¹ with the main different in the dihedral angles of ∠H(3)-O(2)-N(8)-O(1) (22.4° for IMW1c; -159.1° for IMW2c) and ∠O(9)-O(4)-H(3)-O(2) (-61.0° for IMW1c; -4.7° for IMW2c). After the complexes IMW1c and IMW2c, the reaction of Channel RW1c and RW2c respectively went on through elementary reactions TSW1c and TSW2c to form complex IMFW1c and IMFW2c. Transition state TSW1c and TSW2c laid 11.60 and 8.33 kcal·mol⁻¹ respectively above the NO₂···H₂O+HO₂ reactants. All these two elementary processes involved a direct hydrogen abstraction mechanism similar to the reaction without water, as described in Fig. 1. Transition states TSW1c and TSW2c differentiated from each other in the dihedral angles of ∠H(3)-O(2)-N(8)-O(1) and ∠O(9)-O(4)-H(3)-O(2) as described for the prereactive complexes IMW1c and IMW2c. Compared with Channels RW1b and RW2b in Fig. 4, the barrier heights of Channels RW1c and RW2c were only changed by 0.65-1.58 kcal·mol⁻¹, respectively, indicating that, for water-catalyzed channel R1 and R2, Channel RW1c and RW2c is also favorable.

Regarding to the Channel RW3c shown in Fig. 6(c), beginning with the NO₂···H₂O+HO₂ reactants, the reaction progressed through the transition states TSW3c and TSW3c1, undergoing a direct hydrogen abstraction process by the N atom of NO₂ moiety in the NO₂···H₂O complex abstracted the H atom of HO₂ radical. From an energetic point of view, outlined in Fig. 6 and Table S5, the relative energies of the transition state TSW3c and TSW3c1 was 9.38 and 9.35 kcal·mol⁻¹ above the NO₂···H₂O+HO₂ reactants, which was ~ 1.20 kcal·mol⁻¹ less than the relative energies associated with the transition state TSW3b involved in Channel RW3b. This suggests that Channel RW3c was energetically feasible for water-catalyzed HNO₂+³O₂ formation.

As a result of the above findings of ³O₂ formation with a water molecule, the channels occurring through the HO₂···H₂O + NO₂ and NO₂···H₂O+HO₂ reactants may be of great atmospheric relevance, whereas channels occurring through H₂O ···NO₂ +HO₂ reactants may be negligible due to the high barrier heights. Besides, the reaction between HO₂···H₂O and NO₂ leading to the formation of HNO₃+H₂O₂ (Channel RW4) is a new mechanism for the gas-phase formation of HNO₃, though its barrier height is highest in water-catalyzed channels for hydrogen abstraction of NO₂+HO₂ reaction.

3.3 Reaction kinetics

Beyond the mechanisms presented above, another goal of this work was to describe the effect of one water molecule on the formation of $^3\text{O}_2$ from the $\text{NO}_2 + \text{HO}_2$ reaction under atmospheric conditions. To meet this goal, Table 2-Table 4 show the calculated rate constants for different conditions of the title reaction without and with water. More detailed information regarding the different values of the rate constants obtained for the title reaction without and with water can be found in the Supporting Information (Table S6–Table S8†). The title reaction of $^3\text{O}_2$ formation without and with water all began with the formation of a prereactive complex before progressing through the transition state, which is depicted in equation (8).



Assuming that the prereactive complex was in equilibrium with the reactants and was at steady state, the overall rate constant was expressed as

$$k = \frac{k_1}{k_{-1} + k_2} k_2 \quad (9)$$

If $k_2 \ll k_{-1}$, the rate constant was rewritten as

$$k = \frac{k_1}{k_{-1} + k_2} k_2 = K_{\text{eq}} k_2 \quad (10)$$

where K_{eq} and k_2 were given by equation (11) and the VKLab program^[34], respectively.

$$K_{\text{eq}}(T) = \sigma \frac{Q_{\text{CR}}}{Q_{\text{R1}} Q_{\text{R2}}} \exp\left(\frac{E_{\text{R}} - E_{\text{CR}}}{RT}\right) \quad (11)$$

The various Q values denoted the partition functions of the intermediates, reactants NO_2 and HO_2 . E_{R} , E_{CR} are the total energies of the reactants and the post-reactant complex CR; σ is the symmetry number.

For the reaction without water, Table 2 shows that the computed rate constants for Channel R2 (k_{R2}) and Channel R3 (k_{R3}) were respectively 2.26×10^{-16} – 1.95×10^{-15} and 4.09×10^{-16} – 3.66×10^{-15} $\text{cm}^3 \cdot \text{molecule}^{-1} \cdot \text{s}^{-1}$ in the temperature range of 240.0–425.0 K, which was 20–76.8 and 36.2–144 times than the corresponding value of Channel R1 (k_{R1}), showing

that the overall rate constant without water (k_R) in the calculated temperature is main dependent on the Channels R2(*cis*-HONO+O₂ formations) and R3(HNO₂+O₂ formations). At 298 K, the calculated value of k_R was $2.01 \times 10^{-15} \text{ cm}^3 \cdot \text{molecule}^{-1} \cdot \text{s}^{-1}$, which was in good agreement with experimental reports^[42, 43].

For the reaction with water, as pointed out in Table 3, the rate constants of reaction channels occurring through HO₂··H₂O + NO₂ (Channel RWb, k_{RWb}) and NO₂··H₂O+HO₂ (Channel RWc, k_{RWc}) reactants with one water molecule was much larger than that the corresponding value of reaction channels occurring through HO₂··H₂O + NO₂ reaction (Channel RWa, k_{RWa}), showing that the reaction channels occurring through HO₂··H₂O + NO₂ and NO₂··H₂O+HO₂ reactants were most possibly taken places under atmospheric conditions for water-catalyzed NO₂+ HO₂ reaction. Table 3 also shows that, for the title reaction with one water molecule, the values of k_{RWb} and k_{RWc} were significantly faster than the corresponding values (k_R) computed for the naked reaction in the temperature range of 240.0–425.0 K, given that the ratio of k_{RWb}/k_R and k_{RWc}/k_R was 8.27×10^4 – 4.81×10^6 and 2.89×10^1 – 4.71×10^4 , respectively. These findings suggest that, for water-catalyzed ³O₂ formation, water molecule plays an important role in increasing the rate for ³O₂ formation occurring through HO₂··H₂O + NO₂ (Channel RWb) and NO₂··H₂O+HO₂ (Channel RWc) reactions. Besides, the values of k_{RW2b} and k_{RW3b} were significantly faster than the corresponding values (k_{RW1b}) in the calculated temperature range given that the ratio of k_{RW2b}/k_{RW1b} and k_{RW3b}/k_{RW1b} was 1.68×10^1 – 1.22×10^4 and 4.05×10^1 – 9.00×10^1 , respectively, showing that water-catalyzed HO₂··H₂O + NO₂ (Channel RWb, k_{RWb}) reaction mainly occurs through the channels of *trans*-HONO and HNO₂ formations. The result can also be obtained in water-catalyzed NO₂··H₂O+HO₂ (Channel RWc, k_{RWc}), in which the ratio of k_{RW2c}/k_{RW1c} and k_{RW3c}/k_{RW1c} was respectively 3.61 – 1.09×10^2 and 1.77×10^1 – 3.04×10^1 . These results above indicate that, water-catalyzed the *trans*-HONO and HNO₂ formations are obvious than that of *cis*-HONO formation.

To obtain a more complete understanding of the effects of water vapor on the NO₂ + HO₂ reaction, it is necessary to compare the effective rates of the naked and water-catalyzed reactions. The rate for the naked reaction was written as

$$v_{R1} = k_{R1} [\text{NO}_2] [\text{HO}_2] \quad (12)$$

while the rate for water-catalyzed ³O₂ formation via Channels RWb and RWc was respectively

written as

$$v_{\text{RWb}} = k_{\text{RWb}} [\text{HO}_2 \cdots \text{H}_2\text{O}] [\text{NO}_2] = k'_{\text{RWb}} [\text{NO}_2] [\text{HO}_2] \quad (13)$$

$$v_{\text{RWc}} = k_{\text{RWc}} [\text{NO}_2 \cdots \text{H}_2\text{O}] [\text{HO}_2] = k'_{\text{RWc}} [\text{NO}_2] [\text{HO}_2] \quad (14)$$

In these equations, $k'_{\text{RWb}} = k_{\text{RWb}} K_{\text{eq}}(\text{HO}_2 \cdots \text{H}_2\text{O}) [\text{H}_2\text{O}]$, and $k'_{\text{RWc}} = k_{\text{RWc}} K_{\text{eq}}(\text{NO}_2 \cdots \text{H}_2\text{O}) [\text{H}_2\text{O}]$. $[\text{H}_2\text{O}]$ was the concentration of water vapor^[44]. Table 4 shows that the effective rate constants of Channel RWb (k'_{RWb}) are much larger than the corresponding effective rate constant of Channel RWc (k'_{RWc}) within the temperature range of 240.0–425.0 K, indicating that the catalytic effect of Channel RWb on the formation of $^3\text{O}_2$ is much more important than that of Channel RWc. At 298 K, the effective rate constant of Channel RWb is $2.37 \times 10^{-15} \text{ cm}^3 \cdot \text{molecules}^{-1} \cdot \text{s}^{-1}$, which is larger by 1.18 times than the rate constant without water, indicating that water molecule plays an obvious positive effect on enhancing the rate of HONO formation under atmospheric conditions. This result is also agreement with the predication reported by Li et al^[23].

To further quantitatively assess the impact of one water vapor on the formation of $^3\text{O}_2$ in $\text{NO}_2 + \text{HO}_2$ reaction, the total rate constant, k_{tot} , was taken into account as equation (15), which is plotted alongside k_{R} , k'_{RWb} and k'_{RWc} .

$$k_{\text{tot}} = k_{\text{R}} + k'_{\text{RWb}} + k'_{\text{RWc}} \quad (15)$$

The results in Table 4 is estimated that at low temperature, such as 240 K the enhancement factor of Channel RWc is only 0.0005%, which is much smaller than that of Channel RWb, indicating that at low temperatures, positive water vapor effect mainly contributes by Channel RWb (4.47%). While at high temperature, such as 425 K, the positive water vapor effect of Channel RWb and RWc respectively enhances up to 84.5% and 15.5%, showing at high temperatures the positive water effect of both Channel RWb and Channel RWc is obvious under atmospheric conditions.

4. Summary and Conclusions

The effect of a single water molecule on the hydrogen abstraction reaction between NO_2 and HO_2 has been investigated the assisted and unassisted reactions. The reaction without water primarily occurred on triplet potential energy surfaces, and three kinds of reaction channels were identified on triplet potential energy surfaces depending on how the HO_2 radical approached NO_2 , corresponding to the formation of *trans*-HONO+ $^3\text{O}_2$, *cis*-HONO+ $^3\text{O}_2$

and $\text{HNO}_2 + {}^3\text{O}_2$. In accordance with the result of Staikova et al.^[22], the Channels of the formation of *cis*-HONO+ ${}^3\text{O}_2$ and $\text{HNO}_2 + {}^3\text{O}_2$ is easily taken place for the title reaction when a water molecule was not present with the branching ratio of 34.9% and 64.2% at 298 K.

With the inclusion of water there are three significant entrance channels, namely, $\text{H}_2\text{O} \cdots \text{HO}_2 + \text{NO}_2$, $\text{HO}_2 \cdots \text{H}_2\text{O} + \text{NO}_2$ and $\text{NO}_2 \cdots \text{H}_2\text{O} + \text{HO}_2$, that are almost degenerate on the formation of *trans*-HONO+ ${}^3\text{O}_2$, *cis*-HONO+ ${}^3\text{O}_2$ and $\text{HNO}_2 + {}^3\text{O}_2$. As a result of the findings of ${}^3\text{O}_2$ formation with a water molecule, the channels occurring through the $\text{HO}_2 \cdots \text{H}_2\text{O} + \text{NO}_2$ and $\text{NO}_2 \cdots \text{H}_2\text{O} + \text{HO}_2$ reactants may be of great atmospheric relevance, whereas channels occurring through $\text{H}_2\text{O} \cdots \text{NO}_2 + \text{HO}_2$ reactants may be negligible due to the high barrier heights and low rate constants. The rate constants of $\text{HO}_2 \cdots \text{H}_2\text{O} + \text{NO}_2 (k_{\text{RWb}})$ and $\text{NO}_2 \cdots \text{H}_2\text{O} + \text{HO}_2 (k_{\text{RWc}})$ reactions were significantly faster than the corresponding values (k_{R}) computed for the naked reaction in the temperature range of 240.0–425.0 K, given that the ratio of $k_{\text{RWb}}/k_{\text{R}}$ and $k_{\text{RWc}}/k_{\text{R}}$ was 8.27×10^4 – 4.81×10^6 and 2.89×10^1 – 4.71×10^4 , respectively, showing that water molecule plays an important role in increasing the rate for ${}^3\text{O}_2$ formation occurring through $\text{HO}_2 \cdots \text{H}_2\text{O} + \text{NO}_2$ and $\text{NO}_2 \cdots \text{H}_2\text{O} + \text{HO}_2$ reactions. Moreover, at low temperature, such as 240 K the enhancement factor of Channel RWc is only 0.0005%, which is much smaller than that of Channel RWb, indicating that at low temperatures, positive water vapor effect mainly contributes by Channel RWb (4.47%). While at high temperature, such as 425 K, the positive water vapor effect of Channel RWb and RWc respectively enhances up to 84.5% and 15.5%, showing at high temperatures the positive water effect of both Channel RWb and Channel RWc is obvious under atmospheric conditions.

Acknowledgments

This work was supported by the National Natural Science Foundation of China (No: 21207081, 21473108), Education department of shaanxi provincial government research project (No: 14JK1154), the Funds of Research Programs of Shaanxi University of Technology (No: SLGQD13(2)-3, SLGQD13(2)-4) and Shandong Provincial Natural Science Foundation, China (No: ZR2012DQ001). The authors thank Professor Donald G. Truhlar for providing the POLYRATE 8.2 program, and we also thank Professor Shiwei Yin for instructing the software and helpful discussions.

References

- [1] J. S. F. R. J. Buszek, J. M. Anglada, *Int Rev Phys Chem*, 2011, **30**, 335-369.
- [2] E. T. Aaltonen and J. S. Francisco, *J. Phys. Chem. A*, 2003, **107**, 1216-1221.
- [3] J. C. Hansen and J. S. Francisco, *ChemPhysChem*, 2002, **3**, 833-840.
- [4] G. J. Frost and V. Vaida, *J. Geophys. Res.*, 1995, **100**, 18803-18809.
- [5] V. Vaida, H. G. Kjaergaard, P. E. Hintze and D. J. Donaldson, *Science*, 2003, **299**, 1566-1568.

- [6] R. J. Buszek, M. Torrent-Sucarrat, J. M. Anglada and J. S. Francisco, *J. Phys. Chem. A*, 2012, **116**, 5821-5829.
- [7] E. Vöhringer-Martinez, B. Hansmann, H. Hernandez, J. S. Francisco, J. Troe and B. Abel, *Science*, 2007, **315**, 497-501.
- [8] B. Long, X. F. Tan, Z. W. Long, Y. B. Wang, D. S. Ren and W. J. Zhang, *J. Phys. Chem. A*, 2011, **115**, 6559-6567.
- [9] D. Stone and D. M. Rowley, *Phys. Chem. Chem. Phys.*, 2005, **7**, 2156-2163.
- [10] R. S. Zhu and M. C. Lin, *Chem. Phys. Lett.*, 2002, **354**, 217-226.
- [11] T. L. Zhang, W. L. Wang, P. Zhang, J. Lu and Y. Zhang, *Phys. Chem. Chem. Phys.*, 2011, **13**, 20794-20805.
- [12] T. Zhang, R. Wang, W. Wang, S. Min, Q. Xu, Z. Wang, C. Zhao and Z. Wang, *Comput. Theor. Chem.*, 2014, **1045**, 135-144.
- [13] R. Simonaitis and J. Heicklen, *J. Phys. Chem.*, 1976, **80**, 1-7.
- [14] R. Simonaitis and J. Heicklen, *J. Phys. Chem.*, 1974, **78**, 653-657.
- [15] R. A. Cox and R. G. Derwent, *J. Photochem*, 1975, **4**, 139-153.
- [16] H. Niki, P. D. Maker, C. M. Savage and L. P. Breitenbach, *Chem. Phys. Lett.*, 1977, **45**, 564-566.
- [17] W. M. Uselman, S. Z. Levine, W. H. Chan, J. G. Calvert and J. H. Shaw, *Chem. Phys. Lett.*, 1978, **58**, 437-440.
- [18] S. P. Sander and M. E. Peterson, *J. Phys. Chem.*, 1984, **88**, 1566-1571.
- [19] S. Aloisio and J. S. Francisco, *J. Phys. Chem. A*, 2000, **104**, 6212-6217.
- [20] M. Staikova, D. J. Donaldson and J. S. Francisco, *J. Phys. Chem. A*, 2002, **106**, 3023-3028.
- [21] H. Stark, S. S. Brown, J. B. Burkholder, M. Aldener, V. Riffault, T. Gierczak and A. R. Ravishankara, *J. Phys. Chem. A*, 2008, **112**, 9296-9303.
- [22] M. Staikova, D. J. Donaldson and J. S. Francisco, *J. Phys. Chem. A*, 2002, **106**, 3023-3028.
- [23] X. Li, F. Rohrer, A. Hofzumahaus, T. Brauers, R. Häsel, B. Bohn, S. Broch, H. Fuchs, S. Gomm, F. Holland, J. Jäger, J. Kaiser, F. N. Keutsch, I. Lohse, K. Lu, R. Tillmann, R. Wegener, G. M. Wolfe, T. F. Mentel, A. Kiendler-Scharr and A. Wahner, *science*, 2014, **344**, 292-296.
- [24] Frisch, M. J.; Trucks, G.W.; Pople, J. A.; et al. Gaussian 09, Revision A.01; Gaussian Inc.: Pittsburgh, PA, 2009.
- [25] Y. S. Lee, S. A. Kucharski and R. J. Bartlett, *J. Chem. Phys.*, 1984, **81**, 5906-5912.
- [26] T. J. T. Lee, P. R., *Int J Quantum Chem*, 1989, **36**, 199-207.
- [27] B. Long, X. F. Tan, Z. W. Long, Y. B. Wang, D. S. Ren and W. J. Zhang, *J Phys Chem A*, **115**, 6559-6567.
- [28] A. Comandini and K. Brezinsky, *J Phys Chem A*, 2011, **115**, 5547-5559.
- [29] R. Dawes, X. G. Wang, A. W. Jasper and T. Carrington, *J Chem Phys*, 2011, **133**.
- [30] J. C. A. Rienstra-Kiracofe, W. D. Schaefer, H. F., *J. Phys. Chem. A*, 2000, **104**, 9823-9840.
- [31] B. C. Garrett and D. G. Truhlar, *J. Chem. Phys.*, 1979, **70**, 1593-1598.
- [32] B. C. Garrett and D. G. Truhlar, *J. Am. Chem. Soc.*, 1979, **101**, 4534-4548.
- [33] B. C. Garrett, D. G. Truhlar, R. S. Grev and A. W. Magnuson, *J. Phys. Chem.*, 1980, **84**, 1730-1748.
- [34] Y. Y. C. Chuang, J. C.; Fast, P. L.; Villa, J.; Hu, W. P.; Liu, Y. P.; Lynch, G. C.; Jackels, C. F.; Nguyen, K.; Gu, M.Z.; Rossi, I.; Coitino, E.; Clayton, S.; Melissas, V.; Steckler, R.; Garrett, B. C.; Isaacson, A. D.; Truhlar, D. G. POLYRATE, Version 8.2, University of Minnesota: Minnesota, 1999.
- [35] J. Gonzalez, M. Torrent-Sucarrat and J. M. Anglada, *Phys. Chem. Chem. Phys.*, 2010, **12**,

2116-2125.

[36] T. L. L. Zhang, G. N. Wang, W. L. Du, Y. M. Li, C. Y. Lu, J., *Comput. Theor. Chem.*, 2012, **991**, 13-21.

[37] W. Zhang, B. Du and Z. Qin, *J. Phys. Chem. A*, 2014, **118**, 4797-4807.

[38] B. Du and W. Zhang, *J. Phys. Chem. A*, 2013, **117**, 6883-6892.

[39] J. Gonzalez, J. M. Anglada, R. J. Buszek and J. S. Francisco, *J. Am. Chem. Soc.*, 2011, **133**, 3345-3353.

[40] Y. M. Luo, S. Ohno, K., *Chem. Phys. Lett.*, 2009, **469**, 57-61.

[41] J. M. Anglada and J. Gonzalez, *Chem. Phys. Chem.*, 2009, **10**, 3034-3045.

[42] G. S. Tyndall, J. J. Orlando and J. G. Calvert, *Environ Sci Technol*, 1995, **29**, 202-206.

[43] C. J. Howard, *J. Chem. Phys.*, 1977, **67**, 5258-5263.

[44] Y. L. Yung, *Photochemistry of planetary atmospheres*, Oxford Univ, Oxford, 1999.

Table 1 Equilibrium Constants of Relevant $\text{H}_2\text{O}\cdots\text{HO}_2$, $\text{HO}_2\cdots\text{H}_2\text{O}$, $\text{NO}_2\cdots\text{H}_2\text{O}$ and $\text{NO}_2\cdots\text{HO}_2$ Complexes^{a,b}

T(K)	$\text{H}_2\text{O}\cdots\text{HO}_2$	$\text{HO}_2\cdots\text{H}_2\text{O}$	$\text{NO}_2\cdots\text{H}_2\text{O}$	$\text{NO}_2\cdots\text{HO}_2$
240	1.06E-17	2.34E-23	2.38E-23	8.59E-24
250	8.57E-18	2.14E-23	2.38E-23	7.16E-24
278	5.77E-18	1.75E-23	2.43E-23	4.69E-24
288	5.67E-18	1.65E-23	2.46E-23	4.13E-24
298	5.23E-18	1.57E-23	2.50E-23	3.69E-24
308	3.86E-18	1.50E-23	2.55E-23	3.32E-24
325	2.13E-18	1.41E-23	2.64E-23	2.84E-24
375	1.86E-18	1.25E-23	2.99E-23	2.02E-24
425	1.34E-18	1.19E-23	3.44E-23	1.62E-24

^aEquilibrium constants in units of $\text{cm}^3\cdot\text{molecule}^{-1}$. ^bAll equilibrium constants were calculated by using energies computed at CCSD(T)/aug-cc-pVTZ level and partition functions obtained at B3LYP/aug-cc-pVTZ level.

Table 2 Rate constants ($\text{cm}^3 \cdot \text{molecules}^{-1} \cdot \text{s}^{-1}$) for main reaction of the $\text{HO}_2 + \text{NO}_2$ reaction within the temperature range of 240.0-425.0 K

T/K	k_{R1}	k_{R2}	k_{R3}	k_{R}
240	2.54E-17	1.95E-15	3.66E-15	5.64E-15
250	2.28E-17	1.57E-15	2.94E-15	4.53E-15
278	1.80E-17	9.39E-16	1.75E-15	2.71E-15
288	1.68E-17	8.07E-16	1.49E-15	2.31E-15
298	1.59E-17	7.02E-16	1.29E-15	2.01E-15
308	1.51E-17	6.18E-16	1.13E-15	1.76E-15
325	1.40E-17	5.06E-16	9.22E-16	1.44E-15
375	1.21E-17	3.15E-16	5.73E-16	9.00E-16
425	1.13E-17	2.26E-16	4.09E-16	6.46E-16

k_{R1} is the rate constant of Channel R1; k_{R2} is the rate constant of Channel R2, and k_{R3} is the rate constant of Channel R3. $k_{\text{R}} = k_{\text{R1}} + k_{\text{R2}} + k_{\text{R3}}$.

Table 3 Rate constants ($\text{cm}^3 \cdot \text{molecules}^{-1} \cdot \text{s}^{-1}$) for a single water-catalyzed $\text{HO}_2 + \text{NO}_2$ reaction within the temperature range of 240.0–425.0 K

T/K	k_{RW1a}	k_{RW2a}	k_{RW3a}	k_{RWa}	k_{RW1b}	k_{RW2b}
240	1.98E-26	1.73E-22	9.12E-32	1.73E-22	1.11E-13	1.35E-09
250	5.18E-26	3.94E-22	2.34E-31	3.94E-22	1.34E-13	6.16E-10
278	8.14E-25	3.81E-21	3.70E-30	3.81E-21	2.97E-13	1.80E-10
288	2.15E-24	8.26E-21	1.03E-29	8.26E-21	4.20E-13	1.53E-10
298	5.64E-24	1.74E-20	2.93E-29	1.74E-20	5.99E-13	1.43E-10
308	1.44E-23	3.58E-20	8.42E-29	3.58E-20	8.78E-13	1.43E-10
325	6.68E-23	1.13E-19	5.09E-28	1.13E-19	1.67E-12	1.63E-10
375	3.57E-21	2.12E-18	8.16E-26	2.12E-18	1.05E-11	3.59E-10
425	9.17E-20	2.22E-17	6.77E-24	2.23E-17	5.33E-11	8.94E-10
T/K	k_{RW3b}	k_{RWb}	k_{RW1c}	k_{RW2c}	k_{RW3c}	k_{RWc}
240	5.42E-12	1.36E-09	1.27E-15	1.39E-13	2.25E-14	1.63E-13
250	8.30E-12	6.24E-10	2.25E-15	1.92E-13	4.91E-14	2.43E-13
278	2.58E-11	2.06E-10	1.15E-14	4.85E-13	3.34E-13	8.31E-13
288	3.78E-11	1.91E-10	2.03E-14	6.74E-13	6.09E-13	1.30E-12
298	5.47E-11	1.98E-10	3.52E-14	9.32E-13	1.07E-12	2.04E-12
308	7.80E-11	2.22E-10	5.99E-14	1.28E-12	1.82E-12	3.16E-12
325	1.39E-10	3.04E-10	1.41E-13	2.16E-12	4.19E-12	6.49E-12
375	6.20E-10	9.90E-10	1.28E-12	8.59E-12	3.25E-11	4.24E-11
425	2.16E-09	3.11E-09	7.65E-12	2.76E-11	1.63E-10	1.98E-10

k_{RW1a} , k_{RW2a} and k_{RW3a} is the rate constant of Channels RW1a, RW2a and RW3a; respectively; k_{RW1b} , k_{RW2b} and k_{RW3b} is the rate constant of Channels RW1b, RW2b and RW3b; respectively; k_{RW1c} , k_{RW2c} and k_{RW3c} is the rate constant of Channels RW1c, RW2c and RW3c; respectively; k_{RWa} ($k_{\text{RWa}} = k_{\text{RW1a}} + k_{\text{RW2a}} + k_{\text{RW3a}}$); k_{RWb} ($k_{\text{RWb}} = k_{\text{RW1b}} + k_{\text{RW2b}} + k_{\text{RW3b}}$) and k_{RWc} ($k_{\text{RWc}} = k_{\text{RW1c}} + k_{\text{RW2c}} + k_{\text{RW3c}}$)

Table 4 Effective rate constant ($\text{cm}^3 \cdot \text{molecule}^{-1} \cdot \text{s}^{-1}$) for the $\text{HO}_2 + \text{H}_2\text{S}$ reaction with water molecule at different heights in the earth atmosphere

T(K)	$[\text{H}_2\text{O}]^a$	k'_{RWb}	k'_{RWc}	$k'_{\text{RWb}} / (k_{\text{R}} + k'_{\text{RWb}} + k'_{\text{RWc}})$	$k'_{\text{RWc}} / (k_{\text{R}} + k'_{\text{RWb}} + k'_{\text{RWc}})$
240	8.29×10^{15}	2.64E-16	3.22E-20	4.47%	0.0005%
250	2.21×10^{16}	2.95E-16	1.28E-19	6.11%	0.003%
278	2.25×10^{17}	8.11E-16	4.54E-18	23.0%	0.13%
288	4.25×10^{17}	1.34E-15	1.36E-17	36.6%	0.37%
298	7.64×10^{17}	2.37E-15	3.90E-17	53.6%	0.83%
308	1.31×10^{18}	4.36E-15	1.06E-16	70.0%	1.70%
325	3.04×10^{18}	1.30E-14	5.21E-16	86.9%	3.48%
375	2.12×10^{19}	2.62E-13	2.69E-14	90.4%	9.28%
425	8.56×10^{19}	3.17E-12	5.83E-13	84.5%	15.5%

$$k'_{\text{RWb}} = k_{\text{RWb}} K_{\text{eq}}(\text{HO}_2 \cdots \text{H}_2\text{O}) [\text{H}_2\text{O}] \text{ and } k'_{\text{RWc}} = k_{\text{RWc}} K_{\text{eq}}(\text{NO}_2 \cdots \text{H}_2\text{O}) [\text{H}_2\text{O}].$$

Figure Captions

Fig. 1 Schematic energy diagrams of the formation of (a) cis-HONO+³O₂; (b) trans-HONO+³O₂ and (c) HNO₂+³O₂ involved in triplet HO₂+NO₂ reaction

Fig. 2 Geometrical parameters for H₂O⋯HO₂, HO₂⋯H₂O, NO₂⋯H₂O and NO₂⋯HO₂ complexes optimized at the B3LYP/aug-cc-pVTZ level of theory

Fig. 3 Schematic energy diagrams of the formation of (a) cis-HONO⋯H₂O+³O₂; (b) trans-HONO⋯H₂O+³O₂ and (c) HNO₂⋯H₂O+³O₂ in the H₂O⋯HO₂+NO₂ reaction

Fig. 4 Schematic energy diagrams of the formation of (a) cis-HONO⋯H₂O+³O₂; (b) trans-HONO⋯H₂O+³O₂ and (c) HNO₂⋯H₂O+³O₂ in the HO₂⋯H₂O+NO₂ reaction

Fig. 5 Schematic energy diagrams of the formation of HNO₃+H₂O₂ in the HO₂⋯H₂O+NO₂ reaction

Fig. 6 Schematic energy diagrams of the formation of (a) cis-HONO⋯H₂O+³O₂; (b) trans-HONO⋯H₂O+³O₂ and (c) HNO₂⋯H₂O+³O₂ in the NO₂⋯H₂O+HO₂ reaction

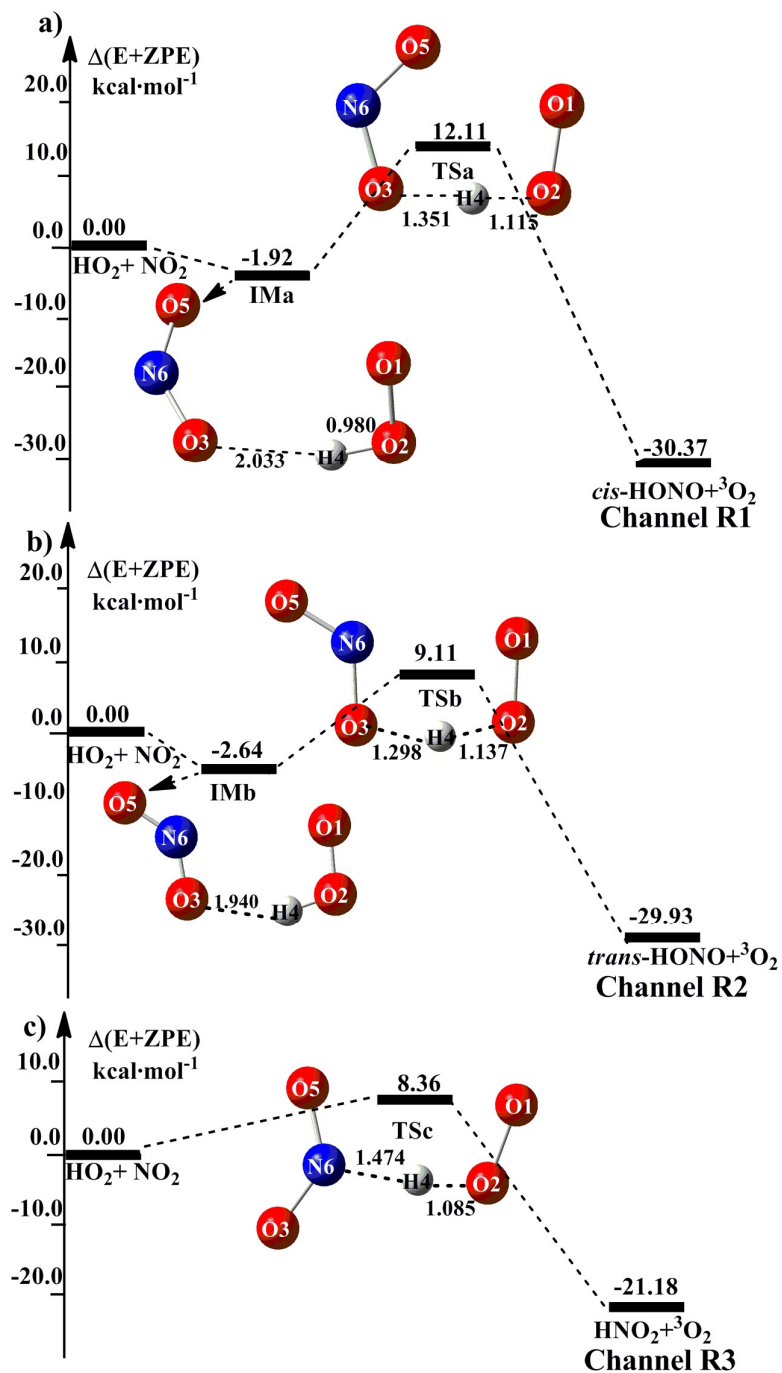


Fig. 1

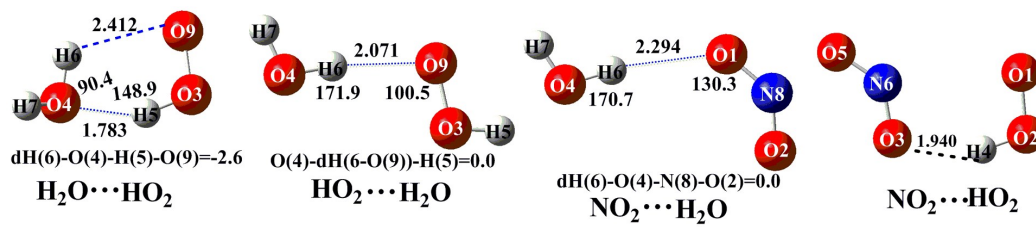


Fig. 2

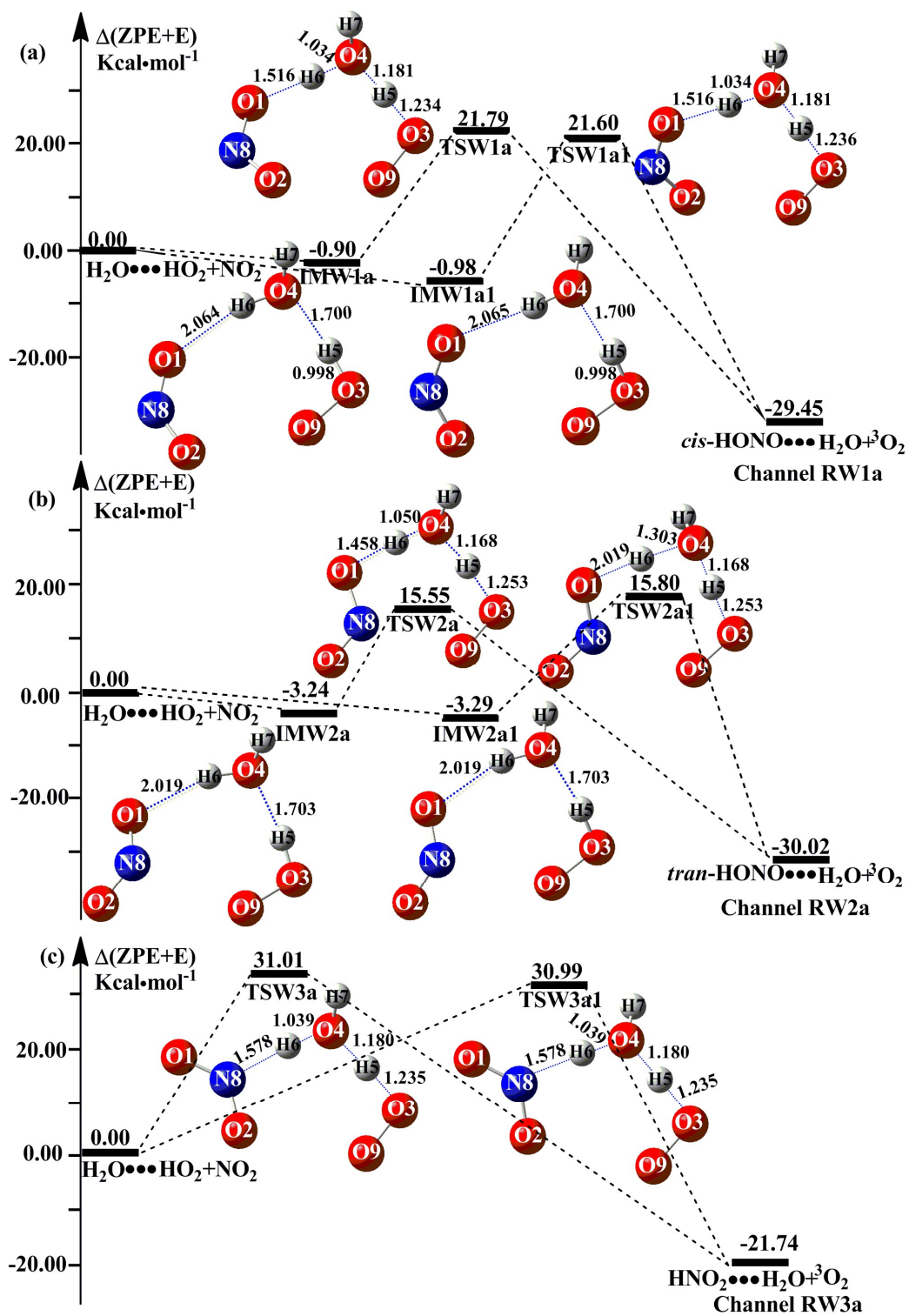


Fig. 3

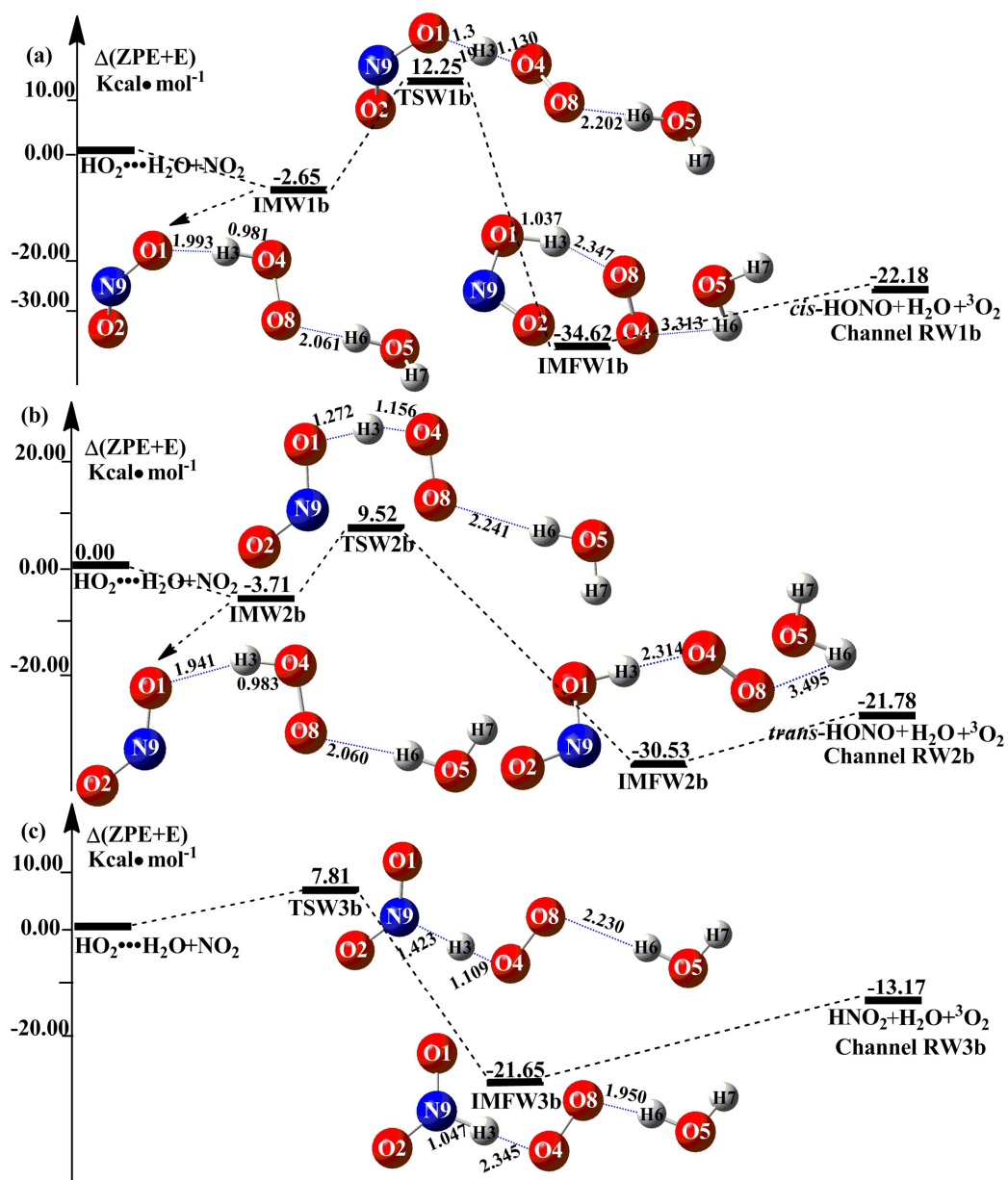


Fig. 4

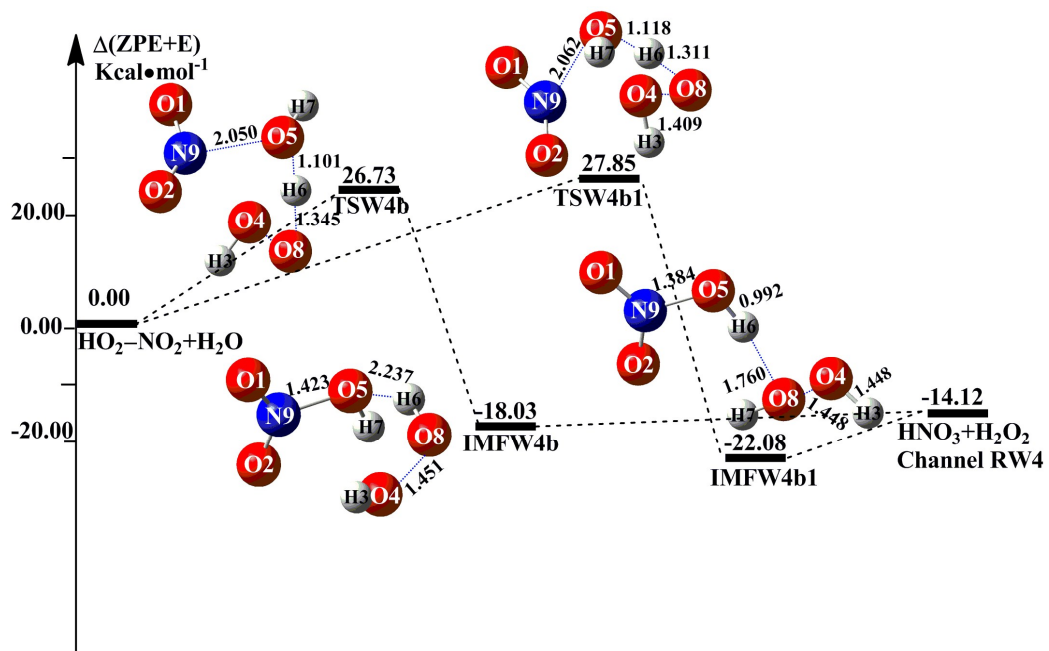


Fig. 5

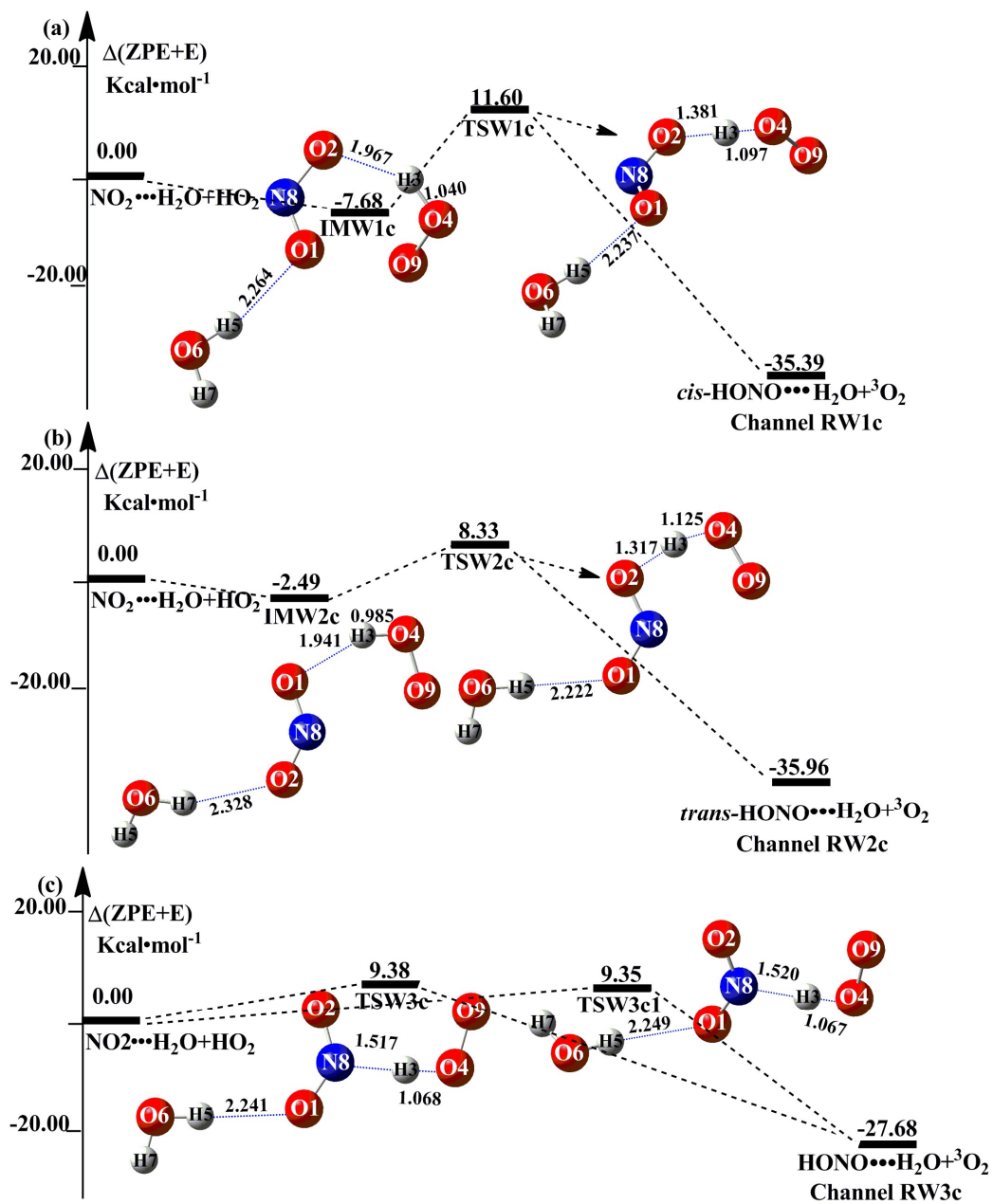


Fig. 6